Simultaneous Beam Training and Target Sensing for RIS-aided Integrated Sensing and Communication

Kangjian Chen *†, Chenhao Qi *† and Octavia A. Dobre ‡
*School of Information Science and Engineering, Southeast University, Nanjing, China
†National Mobile Communications Research Laboratory, Southeast University, Nanjing, China
‡Faculty of Engineering and Applied Science, Memorial University, Canada
Email: {kjchen, qch}@seu.edu.cn, odobre@mun.ca

***Abstract*—In this paper, simultaneous beam training and target sensing for reconfigurable intelligent surface (RIS)-aided integrated sensing and communication (ISAC) systems is investigated. The sensing ability of base station (BS) is exploited to acquire the channel state information of the RIS-aided ISAC. Based on our findings that the energy of the echoes from the RIS can be accumulated in the angle-delay domain while the energy of the echoes from the targets can be accumulated in the Doppler-delay domain, we can distinguish the RIS from the targets. Then we propose a simultaneous beam training and target sensing scheme, which enables the BS to perform the beam training with the RIS and to sense the targets simultaneously based on the mixed echoes from the RIS and the targets, and also enables the user equipment (UE) to perform collaborative sensing to figure out their position. Moreover, the beam alignment between the BS and the UE via the RIS can be directly computed without additional beam training overhead. Simulation results verify the effectiveness of the proposed scheme and show that it outperforms the existing schemes with much smaller training overhead, which benefits from the integration of the sensing units.**

***Index Terms*—Beam training, integrated sensing and communication, reconfigurable intelligent surface, target sensing**

I. Introduction

Wireless communication and radar sensing systems have been developed separately for several decades. With the evolution of technologies, these systems show similarities in several aspects including antenna array, carrier frequency, radio frequency (RF), and signal processing algorithms [1]. On the other hand, many emerging applications, such as autonomous driving and unmanned aerial vehicles, have strong demands for both wireless communication and sensing. Therefore, the numerous similarities and applications have led to the rise of integrated sensing and communication (ISAC) [2]. Earlier works on ISAC intend to explore the coexistence of communication and sensing and focus on mitigating the interference between the communication and the sensing systems while maintaining the communication and sensing functionalities. However, these systems still operate independently, which occupies duplicated hardware and spectral resource. To improve the hardware and the spectral efficiency, more effort is put into integrating the communication and sensing into a single system so that they can sufficiently share various resources. Besides the system level integration, the complementary functionalities of communication and sensing are recently considered to improve the system performance by exploiting the seamless aid from the other functionalities [3].

Another popular topic is the reconfigurable intelligent surface (RIS), which has been proposed to enlarge the signal coverage of the base station (BS) [4]. But one challenge in the RIS-aided systems is the channel state information (CSI) acquisition. When a BS serves multiple user equipments (UEs) with the assistance of RISs, the channel estimation of the BS-RIS-UE link usually requires a large overhead of channel training. To reduce the overhead, it is assumed that all the users share the common channel from the BS to the RIS [5], only one RIS element is activated in each time slot [6], and a multi-directional beam training method for the BS-RIS-UE link is adopted [7].

The low-cost RIS is also exploited to enhance the performance of the ISAC system, which is known as the RIS-aided ISAC system. In [8], it is shown that the RIS can improve the radar detection performance under the communication performance constraints. In [9], the reflection coefficients of the RIS elements are optimized to improve both the sensing and the communication performance.

In this paper, we investigate simultaneous beam training and target sensing for RIS-aided ISAC systems. Based on our findings that the energy of the echoes from the RIS can be accumulated in the angle-delay domain while the energy of the echoes from the targets can be accumulated in the Doppler-delay domain, we can distinguish the RIS from the targets. Then we propose a simultaneous beam training and target sensing scheme, which enables the BS to perform the beam training with the RIS and to sense the targets simultaneously based on the mixed echoes from the RIS and the targets, and also enables the UE to perform collaborative sensing to figure out their position. Moreover, the beam alignment between the BS and the UE via the RIS can be directly computed without additional beam training overhead.

The notations are defined as follows. Symbols for matrices (upper case) and vectors (lower case) are in boldface. $(\cdot)^{\mathrm{T}}$ and $(\cdot)^{\mathrm{H}}$ denote the transpose and conjugate transpose (Hermitian), respectively. $[\boldsymbol{a}]_n$, $[\boldsymbol{A}]_{:,n}$ and $[\boldsymbol{A}]_{m,n}$ denote the nth entry of the vector $\boldsymbol{a}$, the nth column of the matrix $\boldsymbol{A}$ and the

ICC 2023 - IEEE International Conference on Communications | 978-1-5386-7462-8/23/$31.00 ©2023 IEEE | DOI: 10.1109/ICC45041.2023.10279742

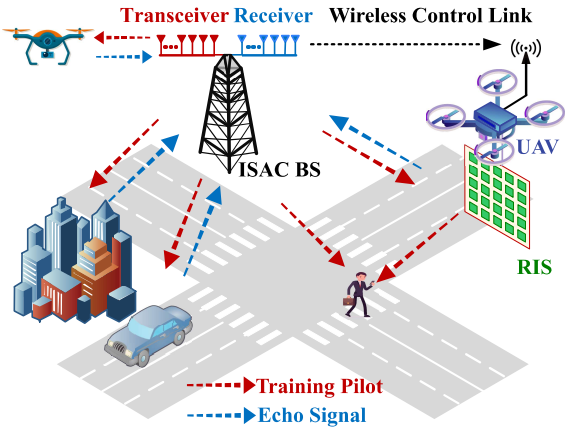

Fig. 1. Illustration of the beam training and target sensing in the ISAC

entry on the mth row and the nth column of the matrix $\boldsymbol{A}$, respectively. $\mathrm{diag}\{\boldsymbol{A}\}$ denotes the diagonal entries of a matrix $\boldsymbol{A}$ and $\mathrm{diag}\{\boldsymbol{a}\}$ denotes the diagonalization operation of a vector $\boldsymbol{a}$. U denotes the uniform random distribution. $\mathrm{sgn}(\cdot)$, $\mathrm{asin}(\cdot)$, and $\mathrm{vec}(\cdot)$ denote the sign function, the arcsine function and the vectorization operation, respectively.

II. System Model

As shown in Fig. 1, we consider an ISAC system, where an ISAC BS serves a UE and detects several targets simultaneously, under the assistance of a RIS. The BS includes a communication transceiver equipped with N_{T} antennas and an echo signal receiver equipped with N_{R} antennas, where the antennas are placed in uniform linear arrays (ULAs) with half wavelength intervals. To reduce the hardware costs, the fully-connected hybrid beamforming is adopted at both the transceiver and the receiver. In this work, we consider the monostatic ISAC scenario, where the transceiver and the receiver are collocated. At the RIS, N_{RIS} RIS elements are deployed for passive reflection and a RIS controller with wireless link to the BS is installed, allowing the BS to control the RIS in real time. For the UE, a half-wavelength-interval ULA with N_{UE} antennas is equipped and the analog beamforming is adopted to form directional beams. Note that although the single-UE scenario is considered for the convenience of expression, the scheme to be proposed can be extended to the multiple-UE scenarios straightforwardly.

We assume the orthogonal frequency division multiplexing (OFDM) with M subcarriers is employed for wideband processing. During the simultaneous beam training and target sensing, the transceiver transmits P OFDM training symbols continuously. Meanwhile, the UE receives the downlink training symbols, and the collocated receiver collects the echoes from the RIS as well as the targets. Then, for the mth subcarrier of the pth symbol, the received signal at the receiver of the BS can be expressed as

$$y_{m,p} = \boldsymbol{v}_p^{\mathrm{H}} \left(\boldsymbol{G}_{\mathrm{R},m} \boldsymbol{\Phi}_p \boldsymbol{G}_{\mathrm{T},m} + \boldsymbol{H}_{\mathrm{r},m}^{(p)} \right) \boldsymbol{f}_p x_{m,p} + \boldsymbol{v}_p^{\mathrm{H}} \boldsymbol{\eta}_{\mathrm{r}}, \quad (1)$$

where $\boldsymbol{v}_p \in \mathbb{C}^{N_{\mathrm{R}} \times 1}$ denotes the analog beamformer at the receiver, $\boldsymbol{G}_{\mathrm{R},m} \in \mathbb{C}^{N_{\mathrm{R}} \times N_{\mathrm{RIS}}}$ denotes the communication channel between the RIS and the receiver, $\boldsymbol{\Phi}_p \triangleq \mathrm{diag}\{[e^{j\phi_1}, e^{j\phi_2}, \cdots, e^{j\phi_{N_{\mathrm{RIS}}}}]^{\mathrm{T}}\}$ denotes the reflection coefficients of the RIS elements, $\boldsymbol{G}_{\mathrm{T},m} \in \mathbb{C}^{N_{\mathrm{RIS}} \times N_{\mathrm{T}}}$ denotes the communication channel between the transceiver and the RIS, $\boldsymbol{H}_{\mathrm{r},m}^{(p)}$ denotes the sensing channel of the T targets, $\boldsymbol{f}_p \in \mathbb{C}^{N_{\mathrm{T}} \times 1}$ denotes the analog beamformer at the transmitter, $x_{m,p}$ denotes the transmit signal, and $\boldsymbol{\eta}_{\mathrm{r}} \sim \mathcal{CN}\left(\boldsymbol{0}, \sigma_{\mathrm{r}}^2 \boldsymbol{I}_{N_{\mathrm{R}}}\right)$ denotes the additive white Gaussian noise (AWGN) vector.

On a parallel branch, for the mth subcarrier of the pth symbol, the received signal at the UE can be expressed as

$$z_{m,p} = \boldsymbol{w}_p^{\mathrm{H}} (\boldsymbol{H}_{\mathrm{c},m} + \widetilde{\boldsymbol{H}}_{\mathrm{c},m} \boldsymbol{\Phi}_p \boldsymbol{G}_{\mathrm{T},m}) \boldsymbol{f}_p x_{m,p} + \boldsymbol{w}_p^{\mathrm{H}} \boldsymbol{\eta}_{\mathrm{c}}, \quad (2)$$

where $\boldsymbol{w}_p \in \mathbb{C}^{N_{\mathrm{UE}} \times 1}$ denotes the analog beamformer, $\boldsymbol{H}_{\mathrm{c},m} \in \mathbb{C}^{N_{\mathrm{UE}} \times N_{\mathrm{T}}}$ denotes the channel between the transceiver and the UE, $\widetilde{\boldsymbol{H}}_{\mathrm{c},m} \in \mathbb{C}^{N_{\mathrm{RIS}} \times N_{\mathrm{UE}}}$ denotes the channel between the RIS and the UE, and $\boldsymbol{\eta}_{\mathrm{c}} \sim \mathcal{CN}\left(\boldsymbol{0}, \sigma_{\mathrm{c}}^2 \boldsymbol{I}_{N_{\mathrm{UE}}}\right)$ denotes the AWGN vector. For the wideband OFDM systems, the frequency-domain communication channel between the transceiver and the RIS at the mth subcarrier can be expressed as [1]

$$\boldsymbol{G}_{\mathrm{T},m} = \sum_{l=1}^{L_{\mathrm{BR}}} \zeta_m^{(l)} \boldsymbol{\alpha}\left(N_{\mathrm{RIS}}, \varphi_{\mathrm{BR}}^{(l)}\right) \boldsymbol{\alpha}\left(N_{\mathrm{T}}, \theta_{\mathrm{BR}}^{(l)}\right)^{\mathrm{H}}, \quad (3)$$

where $\zeta_m^{(l)} \triangleq g_{\mathrm{BR}}^{(l)} e^{-j2\pi(m-1)\tau_{\mathrm{BR}}^{(l)}\Delta f}$, $g_{\mathrm{BR}}^{(l)}$, $\tau_{\mathrm{BR}}^{(l)}$, $\varphi_{\mathrm{BR}}^{(l)}$ and $\theta_{\mathrm{BR}}^{(l)}$ denote the channel gain, the channel delay, the channel angle-of-arrival (AoA) and the channel angle-of-departure (AoD) of the lth path, respectively. L_{BR} denotes the number of paths, and Δf denotes the subcarrier spacing. $\tau_{\mathrm{BR}}^{(l)} = r_{\mathrm{BR}}^{(l)}/c$, where $r_{\mathrm{BR}}^{(l)}$ denotes the distance of the lth path from the transceiver to the RIS and c denotes the speed of light. The function $\boldsymbol{\alpha}(\cdot)$ denotes the steering vector and can be expressed as

$$\boldsymbol{\alpha}(N, \theta) = \frac{1}{\sqrt{N}} [1, e^{j\pi\theta}, \cdots, e^{j(N-1)\pi\theta}]^{\mathrm{T}}. \quad (4)$$

According to the channel reciprocity, the frequency-domain communication channel between the receiver and the RIS at the mth subcarrier can be expressed as

$$\boldsymbol{G}_{\mathrm{R},m} = \sum_{l=1}^{L_{\mathrm{BR}}} \zeta_m^{(l)} \boldsymbol{\alpha}\left(N_{\mathrm{R}}, \theta_{\mathrm{BR}}^{(l)}\right) \boldsymbol{\alpha}\left(N_{\mathrm{RIS}}, \varphi_{\mathrm{BR}}^{(l)}\right)^{\mathrm{T}}. \quad (5)$$

Similarly, for the wideband OFDM systems, the frequency-domain communication channel between the transceiver and the UE at the mth subcarrier can be expressed as

$$\boldsymbol{H}_{\mathrm{c},m} = \sum_{l=1}^{L_{\mathrm{BU}}} \chi_m^{(l)} \boldsymbol{\alpha}\left(N_{\mathrm{UE}}, \varphi_{\mathrm{BU}}^{(l)}\right) \boldsymbol{\alpha}\left(N_{\mathrm{T}}, \theta_{\mathrm{BU}}^{(l)}\right)^{\mathrm{H}}, \quad (6)$$

where $\chi_m^{(l)} \triangleq g_{\mathrm{BU}}^{(l)} e^{-j2\pi(m-1)\tau_{\mathrm{BU}}^{(l)}\Delta f}$, $g_{\mathrm{BU}}^{(l)}$, $\tau_{\mathrm{BU}}^{(l)}$, $\varphi_{\mathrm{BU}}^{(l)}$ and $\theta_{\mathrm{BU}}^{(l)}$ denote the channel gain, the channel delay, the channel AoA and the channel AoD of the lth path, respectively. $\tau_{\mathrm{BU}}^{(l)} = r_{\mathrm{BU}}^{(l)}/c$, where $r_{\mathrm{BU}}^{(l)}$ denotes the distance of the lth path from the transceiver to the UE. The sensing channel of targets can be expressed as

$$\boldsymbol{H}_{\mathrm{r},m}^{(p)} = \sum_{l=1}^{T} \gamma_{m,p}^{(l)} \boldsymbol{\alpha}\left(N_{\mathrm{R}}, \theta_{\mathrm{Tar}}^{(l)}\right) \boldsymbol{\alpha}\left(N_{\mathrm{T}}, \theta_{\mathrm{Tar}}^{(l)}\right)^{\mathrm{H}}, \quad (7)$$

where T denotes the number of targets, $\gamma_{m,p}^{(l)} \triangleq g_{\mathrm{Tar}}^{(l)} e^{-j2\pi(m-1)\tau_{\mathrm{Tar}}^{(l)}\Delta f} e^{j2\pi(p-1)f_{\mathrm{Tar}}^{(l)}T_{\mathrm{s}}}$, $g_{\mathrm{Tar}}^{(l)}$, $\tau_{\mathrm{Tar}}^{(l)}$, $f_{\mathrm{Tar}}^{(l)}$ and $\theta_{\mathrm{Tar}}^{(l)}$ denote the channel gain, the channel delay, the Doppler frequency and the channel AoD of the lth target, respectively. T_{s} denotes the duration of the OFDM symbol. $\tau_{\mathrm{Tar}}^{(l)} = 2r_{\mathrm{Tar}}^{(l)}/c$, where $r_{\mathrm{Tar}}^{(l)}$ denotes the distance from the transceiver to the lth target. $f_{\mathrm{Tar}}^{(l)} = 2v_{\mathrm{Tar}}^{(l)}/\lambda$, where $v_{\mathrm{Tar}}^{(l)}$ denotes the radial velocity of the lth target and λ denotes the wavelength of the carrier frequency.

To support high-speed transmission, beam alignment among the BS, the RIS and the UE is needed. One way to achieve high-quality beam alignment is the codebook-based beam training [10], [11]. Generally, two parts of beam training, including the beam training for the BS-UE link and the beam training for the BS-RIS-UE link, are needed to achieve beam alignment between the BS, the RIS and the UE. To reveal the inherent shortcomings of the conventional beam training method, we take the beam training for the BS-RIS-UE link as an example. The codebooks for the BS, the RIS and the UE can be expressed as $\boldsymbol{\mathcal{B}} = \{\boldsymbol{b}_1, \boldsymbol{b}_2, \cdots, \boldsymbol{b}_{N_{\mathrm{T}}}\}$, $\boldsymbol{\mathcal{R}} = \{\boldsymbol{r}_1, \boldsymbol{r}_2, \cdots, \boldsymbol{r}_{N_{\mathrm{RIS}}}\}$ and $\boldsymbol{\mathcal{U}} = \{\boldsymbol{u}_1, \boldsymbol{u}_2, \cdots, \boldsymbol{u}_{N_{\mathrm{UE}}}\}$, respectively, where

$$\begin{aligned}
&\boldsymbol{b}_n = \boldsymbol{\alpha}(N_{\mathrm{T}}, (2n-2)/N_{\mathrm{T}}),\ n = 1, 2, \cdots, N_{\mathrm{T}},\\
&\boldsymbol{r}_s = \sqrt{N_{\mathrm{RIS}}}\boldsymbol{\alpha}(N_{\mathrm{RIS}}, (2s-2)/N_{\mathrm{RIS}}),\ s = 1, 2, \cdots, N_{\mathrm{RIS}},\\
&\boldsymbol{u}_t = \boldsymbol{\alpha}(N_{\mathrm{UE}}, (2t-2)/N_{\mathrm{UE}}),\ t = 1, 2, \cdots, N_{\mathrm{UE}}. \qquad (8)
\end{aligned}$$

The existing works focus on (2) and perform the beam alignment for the BS-RIS-UE link via

$$\begin{aligned}
&\max_{\boldsymbol{w}_p, \boldsymbol{\Phi}_p, \boldsymbol{f}_p} \left|\boldsymbol{w}_p^{\mathrm{H}} \boldsymbol{\Phi}_p \boldsymbol{G}_{\mathrm{T},m} \boldsymbol{f}_p\right|^2\\
&\quad \text{s.t.} \quad \boldsymbol{w}_p \in \boldsymbol{\mathcal{U}},\ \mathrm{diag}\{\boldsymbol{\Phi}_p\} \in \boldsymbol{\mathcal{R}},\ \boldsymbol{f}_p \in \boldsymbol{\mathcal{B}}. \qquad (9)
\end{aligned}$$

To solve (9), we need to test all the codewords in $\boldsymbol{\mathcal{B}}$, $\boldsymbol{\mathcal{R}}$ and $\boldsymbol{\mathcal{U}}$ one by one. Totally $N_{\mathrm{T}}N_{\mathrm{RIS}}N_{\mathrm{UE}}$ times of beam training are needed, which is much larger than the $N_{\mathrm{T}}N_{\mathrm{UE}}$ times of beam training for the conventional BS-UE link. Novel beam training method for the BS-RIS-UE link with low training overhead is needed. On the other hand, in the emerging ISAC systems, the BS is endowed with the ability of sensing, which brings tremendous vitality to the existing communication systems. It would be interesting to investigate how to exploit the sensing ability of the BS for reducing the training overhead of the BS-RIS-UE link, which will be discussed in the next section.

For conventional beam training, beam alignment is performed to determine the best beam pair between the transmitter and the receiver. As a result, the transmitter needs to transmit multiple pilots with the same beamforming vector so that the receiver can test the codewords in its codebook sequentially. On the other hand, during the target sensing, the transmitter also needs to transmit continuous waveform with the same beamforming vector so that the Doppler effects can be exploited to identify the moving targets. The similarity between the beam training and target sensing implies that we may reuse the downlink training beams and pilots for target sensing, which will be detailed in the next section.

III. Simultaneous Beam Training and Target Sensing

In this section, we propose a simultaneous beam training and target sensing scheme for the RIS-aided ISAC systems. For the beam training, we aim to exploit the sensing ability of the ISAC BS to reduce the training overhead for the RIS-aided communication systems. For the target sensing, we aim to reuse the training pilots to identify the moving targets.

A. Beam training for the BS-RIS-BS link

Different from the existing works that focus on (2) and perform beam training for the BS-RIS-UE link via solving (9), we first turn to the BS-RIS-BS link contained in (1) and perform the beam alignment between BS and RIS via

$$\begin{aligned}
&\max_{\boldsymbol{\Phi}_p, \boldsymbol{f}_p} \left|\boldsymbol{v}_p^{\mathrm{H}} \boldsymbol{G}_{\mathrm{R},m} \boldsymbol{\Phi}_p \boldsymbol{G}_{\mathrm{T},m} \boldsymbol{f}_p\right|^2\\
&\quad \text{s.t.} \quad \mathrm{diag}\{\boldsymbol{\Phi}_p\} \in \boldsymbol{\mathcal{R}},\ \boldsymbol{f}_p \in \boldsymbol{\mathcal{B}}, \boldsymbol{v}_p = \boldsymbol{\alpha}(N_{\mathrm{R}}, \Xi(\boldsymbol{f}_p)), \qquad (10)
\end{aligned}$$

where $\Xi(\cdot)$ denotes the spatial direction of a steering vector, for example, $\Xi(\boldsymbol{\alpha}(N, \theta)) = \theta$. To solve (10), we test all the codewords in $\boldsymbol{\mathcal{B}}$ as well as $\boldsymbol{\mathcal{R}}$ one by one, and only $N_{\mathrm{T}}N_{\mathrm{RIS}}$ times of beam training are needed thanks to the channel reciprocity between the BS-RIS link and the RIS-BS link. When testing the nth codeword in $\boldsymbol{\mathcal{B}}$ and the sth codeword in $\boldsymbol{\mathcal{R}}$, the received signal at the receiver can be expressed as

$$y_{m,p} = \boldsymbol{v}_n^{\mathrm{H}}(\boldsymbol{G}_{\mathrm{R},m}\mathrm{diag}\{\boldsymbol{r}_s\}\boldsymbol{G}_{\mathrm{T},m} + \boldsymbol{H}_{\mathrm{r},m}^{(p)})\boldsymbol{b}_n + \boldsymbol{v}_n^{\mathrm{H}}\boldsymbol{\eta}_{\mathrm{r}}, \quad (11)$$

where $n \in \{1, 2, \cdots N_{\mathrm{T}}\}$, $s \in \{1, 2, \cdots, N_{\mathrm{RIS}}\}$, $\boldsymbol{v}_n = \boldsymbol{\alpha}(N_{\mathrm{R}}, \Xi(\boldsymbol{u}_n))$ and $p = (n-1)N_{\mathrm{RIS}} + s$. Note that we set $x_{m,p} = 1$ in (11). When testing each codeword in $\boldsymbol{\mathcal{B}}$, N_{RIS} codewords in $\boldsymbol{\mathcal{R}}$ are tested sequentially. For the test of the nth codeword in $\boldsymbol{\mathcal{B}}$, we stack the N_{RIS} times of receptions at the M subcarriers together as $\boldsymbol{Y}_n \in \mathbb{C}^{N_{\mathrm{RIS}} \times M}$. Then, we have

$$\begin{aligned}
\boldsymbol{Y}_n = &\sum_{i=1}^{L_{\mathrm{BR}}}\sum_{k=1}^{L_{\mathrm{BR}}} \mu_{i,k}\boldsymbol{F}_{N_{\mathrm{RIS}}}\boldsymbol{\alpha}\left(N_{\mathrm{RIS}}, \varphi_{\mathrm{BR}}^{(i)} + \varphi_{\mathrm{BR}}^{(k)}\right)\boldsymbol{e}_{i,k}^{\mathrm{T}} + \boldsymbol{N}_n\\
&+\sum_{l=1}^{T}\kappa_l\boldsymbol{\alpha}\left(N_{\mathrm{RIS}}, 2f_{\mathrm{Tar}}^{(l)}T_{\mathrm{s}}\right)\boldsymbol{\alpha}\left(M, -2\tau_{\mathrm{Tar}}^{(l)}\Delta f\right)^{\mathrm{T}} \qquad (12)
\end{aligned}$$

where

$$\begin{aligned}
&\mu_{i,k} = g_{\mathrm{BR}}^{(i)}g_{\mathrm{BR}}^{(k)}\boldsymbol{v}_n^{\mathrm{H}}\boldsymbol{\alpha}\left(N_{\mathrm{R}}, \theta_{\mathrm{BR}}^{(k)}\right)\boldsymbol{\alpha}\left(N_{\mathrm{T}}, \theta_{\mathrm{BR}}^{(i)}\right)^{\mathrm{H}}\boldsymbol{b}_n,\\
&\kappa_l = \sqrt{MN_{\mathrm{RIS}}}g_{\mathrm{Tar}}^{(l)}\boldsymbol{v}_n^{\mathrm{H}}\boldsymbol{\alpha}\left(N_{\mathrm{R}}, \theta_{\mathrm{Tar}}^{(l)}\right)\boldsymbol{\alpha}\left(N_{\mathrm{T}}, \theta_{\mathrm{Tar}}^{(l)}\right)^{\mathrm{H}}\boldsymbol{b}_n,\\
&\boldsymbol{F}_{N_{\mathrm{RIS}}} = [\boldsymbol{r}_1, \boldsymbol{r}_2, \cdots, \boldsymbol{r}_{N_{\mathrm{RIS}}}]^{\mathrm{T}},\\
&\boldsymbol{e}_{i,k} = \sqrt{M}\boldsymbol{\alpha}\left(M, -2\left(\tau_{\mathrm{BR}}^{(i)} + \tau_{\mathrm{BR}}^{(k)}\right)\Delta f\right), \qquad (13)
\end{aligned}$$

and $\boldsymbol{N}_n$ is the stack of noise terms.

Note that both $\boldsymbol{e}_{i,k}$ and $\boldsymbol{\alpha}\left(M, -2\tau_{\mathrm{Tar}}^{(l)}\Delta f\right)$ are the steering vectors related to the subcarrier spacing and the channel delay. A regular approach to accumulate the received signals at all subcarriers is the Fourier transform. Define the $M \times M$ inverse discrete fourier transform (IDFT) matrix as $\boldsymbol{F}_M$,

where $[\boldsymbol{F}_M]_{:,m} = \sqrt{M}\boldsymbol{\alpha}(M,(2m-2)/M)$. Postmutiplying $\boldsymbol{Y}_n$ with $\boldsymbol{F}_M$, we can obtain

$$\widetilde{\boldsymbol{Y}}_n = \sum_{i=1}^{L_{\mathrm{BR}}}\sum_{k=1}^{L_{\mathrm{BR}}} \mu_{i,k}\boldsymbol{F}_{N_{\mathrm{RIS}}}\boldsymbol{\alpha}\left(N_{\mathrm{RIS}}, \varphi_{\mathrm{BR}}^{(i)} + \varphi_{\mathrm{BR}}^{(k)}\right)\widetilde{\boldsymbol{e}}_{i,k}^{\mathrm{T}} + \sum_{l=1}^{T}\kappa_l\boldsymbol{\alpha}\left(N_{\mathrm{RIS}}, 2f_{\mathrm{Tar}}^{(l)}T_{\mathrm{s}}\right)\widetilde{\boldsymbol{d}}_l^{\mathrm{T}} + \widetilde{\boldsymbol{N}}_n, \tag{14}$$

where

$$\begin{aligned}
&[\widetilde{\boldsymbol{e}}_{i,k}]_m = G_M\left((2m-2)\pi/M - 2\pi\left(\tau_{\mathrm{BR}}^{(i)} + \tau_{\mathrm{BR}}^{(k)}\right)\Delta f\right),\\
&[\widetilde{\boldsymbol{d}}_l]_m = G_M\left((2m-2)\pi/M - 2\pi\tau_{\mathrm{Tar}}^{(l)}\Delta f\right)/\sqrt{M},\\
&G_M(\psi) \triangleq e^{j(M-1)\psi/2}\sin(M\psi/2)/\sin(\psi/2).
\end{aligned} \tag{15}$$

In (14), the peaks of RIS echoes from different angles locate in different rows of $\widetilde{\boldsymbol{Y}}_n$. In addition, the peaks of echoes from either RIS or targets with different delays locate in different columns of $\widetilde{\boldsymbol{Y}}_n$ regarding the property of $G_M(\psi)$. Therefore, (14) is an expression in the angle-delay domain.

Note that $\boldsymbol{\alpha}\left(N_{\mathrm{RIS}}, 2f_{\mathrm{Tar}}^{(l)}T_{\mathrm{s}}\right)$ in (14) is a steering vector related to the Doppler frequency and the OFDM symbol duration. To accumulate the energy of the echoes from targets over time, we define the $N_{\mathrm{RIS}}\times N_{\mathrm{RIS}}$ DFT matrix as $\boldsymbol{W}_{N_{\mathrm{RIS}}}$, where $[\boldsymbol{W}_{N_{\mathrm{RIS}}}]_{:,n} = \sqrt{N_{\mathrm{RIS}}}\boldsymbol{\alpha}(N_{\mathrm{RIS}},(2-2n)/N_{\mathrm{RIS}})$. Premutiplying $\widetilde{\boldsymbol{Y}}_n$ with $\boldsymbol{W}_{N_{\mathrm{RIS}}}^{\mathrm{T}}/\sqrt{N_{\mathrm{RIS}}}$, we have

$$\overline{\boldsymbol{Y}}_n \overset{(a)}{=} \sum_{i=1}^{L_{\mathrm{BR}}}\sum_{k=1}^{L_{\mathrm{BR}}} \mu_{i,k}\boldsymbol{\alpha}\left(N_{\mathrm{RIS}}, \varphi_{\mathrm{BR}}^{(i)} + \varphi_{\mathrm{BR}}^{(k)}\right)\widetilde{\boldsymbol{e}}_{i,k}^{\mathrm{T}} + \sum_{l=1}^{T}\kappa_l\widetilde{\boldsymbol{c}}_l\widetilde{\boldsymbol{d}}_l^{\mathrm{T}} + \overline{\boldsymbol{N}}_n, \tag{16}$$

where

$$[\widetilde{\boldsymbol{c}}_l]_s = \frac{1}{\sqrt{N_{\mathrm{RIS}}}}G_{N_{\mathrm{RIS}}}\left(2\pi f_{\mathrm{Tar}}^{(l)}T_{\mathrm{s}} - \frac{(2n-2)\pi}{N_{\mathrm{RIS}}}\right), \tag{17}$$

and (a) holds because $\boldsymbol{W}_{N_{\mathrm{RIS}}}^{\mathrm{T}}\boldsymbol{F}_{N_{\mathrm{RIS}}}/\sqrt{N_{\mathrm{RIS}}} = \boldsymbol{I}_{N_{\mathrm{RIS}}}$. The physical meanings of the columns of $\overline{\boldsymbol{Y}}_n$ in (16) are the same as those of $\widetilde{\boldsymbol{Y}}_n$ in (14), while their physical meanings of the rows are different. To be specific, the peaks of echoes from targets with different Doppler frequencies locate in different rows of $\overline{\boldsymbol{Y}}_n$ regarding the property of $G_M(\psi)$. Therefore, (16) is an expression in the Doppler-delay domain.

From (14) and (16), we find that the energy of the echoes from the RIS is accumulated in the angle-delay domain and is dispersed the in Doppler-delay domain, while the energy of the echoes from the targets is accumulated in the Doppler-delay domain and is dispersed in the angle-delay domain. We may use the difference between the properties of the echoes from the RIS and the echoes from the targets to perform beam training and target sensing based on the mixed echoes from the RIS and the targets in (12). Note that the path gains of the non-LoS (NLoS) paths are much smaller than that of the LoS path especially in mmWave or terahertz band. We then focus on analyzing the LoS path, and take the target with the biggest received power as an example at the same time. Define

$$\begin{aligned}
&\widetilde{\boldsymbol{Y}}_n^{(\mathrm{c})} \triangleq \mu_{1,1}\boldsymbol{F}_{N_{\mathrm{RIS}}}\boldsymbol{\alpha}\left(N_{\mathrm{RIS}}, 2\varphi_{\mathrm{BR}}^{(1)}\right)\widetilde{\boldsymbol{e}}_{1,1}^{\mathrm{T}},\\
&\widetilde{Q}^{(\mathrm{c})} \triangleq \max_{s,m}\left|[\widetilde{\boldsymbol{Y}}_n^{(\mathrm{c})}]_{s,m}\right|,\\
&\widetilde{\boldsymbol{Y}}_n^{(\mathrm{r})} \triangleq \kappa_1\boldsymbol{\alpha}\left(N_{\mathrm{RIS}}, 2f_{\mathrm{Tar}}^{(1)}T_s\right)\widetilde{\boldsymbol{d}}_1^{\mathrm{T}}, \widetilde{Q}^{(\mathrm{r})} \triangleq \max_{s,m}\left|[\widetilde{\boldsymbol{Y}}_n^{(\mathrm{r})}]_{s,m}\right|,\\
&\overline{\boldsymbol{Y}}_n^{(\mathrm{c})} \triangleq \mu_{1,1}\boldsymbol{\alpha}\left(N_{\mathrm{RIS}}, 2\varphi_{\mathrm{BR}}^{(1)}\right)\widetilde{\boldsymbol{e}}_{1,1}^{\mathrm{T}}, \overline{Q}^{(\mathrm{c})} \triangleq \max_{s,m}\left|[\overline{\boldsymbol{Y}}_n^{(\mathrm{c})}]_{s,m}\right|,\\
&\overline{\boldsymbol{Y}}_n^{(\mathrm{r})} \triangleq \kappa_1\widetilde{\boldsymbol{c}}_1\widetilde{\boldsymbol{d}}_1^{\mathrm{T}}, \quad \overline{Q}^{(\mathrm{r})} \triangleq \max_{s,m}\left|[\overline{\boldsymbol{Y}}_n^{(\mathrm{r})}]_{s,m}\right|,
\end{aligned} \tag{18}$$

where the first path is termed as the LoS path and the first target is termed as the target with the biggest received power. Suppose $\widetilde{Q}^{(\mathrm{c})} \geq \overline{Q}^{(\mathrm{r})}$, which implies that the accumulated power of the echoes from the RIS in the angle-delay domain is stronger than the accumulated power of the echoes from the targets in the Doppler-delay domain, and then we have

$$\frac{\widetilde{Q}^{(\mathrm{c})}}{\widetilde{Q}^{(\mathrm{r})}} \geq \frac{\widetilde{Q}^{(\mathrm{c})}}{\overline{Q}^{(\mathrm{r})}}\cdot\frac{\overline{Q}^{(\mathrm{r})}}{\widetilde{Q}^{(\mathrm{r})}} \geq \sqrt{N_{\mathrm{RIS}}/2}. \tag{19}$$

Similarly, if $\overline{Q}^{(\mathrm{r})} > \widetilde{Q}^{(\mathrm{c})}$, we have $\overline{Q}^{(\mathrm{r})}/\overline{Q}^{(\mathrm{c})} > \sqrt{N_{\mathrm{RIS}}/2}$. The relation in (19) implies that, if $\widetilde{Q}^{(\mathrm{c})} \geq \overline{Q}^{(\mathrm{r})}$, the dispersed power of the echoes from the target is much smaller than the accumulated power of the echoes from the RIS in angle-delay domain. On the other hand, if $\widetilde{Q}^{(\mathrm{c})} < \overline{Q}^{(\mathrm{r})}$, the dispersed power of the echoes from the RIS is much smaller than the accumulated power of the echoes from the target in Doppler-delay domain. Without loss of generality, we assume $\widetilde{Q}^{(\mathrm{c})} \geq \overline{Q}^{(\mathrm{r})}$ and the case when $\widetilde{Q}^{(\mathrm{c})} < \overline{Q}^{(\mathrm{r})}$ can be easily extended. Based on (19), we focus on the processing in angle-delay domain and omit the interference of targets, and then the results of beam alignment for the BS-RIS-BS link can be obtained via

$$(n_{\mathrm{RIS}}^*, s_{\mathrm{RIS}}^*, m_{\mathrm{RIS}}^*) = \arg\max_{n,s,m}\left|[\widetilde{\boldsymbol{Y}}_n]_{s,m}\right|, \tag{20}$$

where $n \in \{1,2,\cdots,N_{\mathrm{T}}\}$, $s \in \{1,2,\cdots,N_{\mathrm{RIS}}\}$, $m \in \{1,2,\cdots,M\}$, n_{RIS}^* denotes the index of the best beam in $\boldsymbol{\mathcal{B}}$, s_{RIS}^* denotes the index of the best beam in $\boldsymbol{\mathcal{R}}$, and m_{RIS}^* denotes the index of the column of $\boldsymbol{F}_M$ best fit for the distance between the RIS and the BS. Note that the estimation accuracy in (20) is limited by the DFT resolution. To improve the estimation accuracy, we extend the method for AoD estimation in [12] to a more general case. We define an $N\times N$ DFT matrix $\boldsymbol{W}_N$. For $\boldsymbol{g} = \boldsymbol{\alpha}(N,\theta)$, we define $\widetilde{\boldsymbol{g}} \triangleq \boldsymbol{W}_N\boldsymbol{g}$. Suppose $g^* = \arg\max_g|[\widetilde{\boldsymbol{g}}]_g|$ and $\widetilde{g}^* = \arg\max_{g,g\neq g^*}|[\widetilde{\boldsymbol{g}}]_g|$. Then, the estimation of θ can be expressed as [12]

$$\widehat{\theta} = \left(-1 + \frac{\widetilde{g}^* + g^*}{N}\right) - \frac{1}{\pi}\mathrm{asin}\left(\frac{\Gamma\sin(\delta) - \Gamma\sqrt{1-\Gamma^2}\sin(\delta)\cos(\delta)}{\sin(\delta)^2 + \Gamma^2\cos(\delta)^2}\right) \tag{21}$$

where $\delta = \pi/N$ and $\Gamma = \mathrm{sgn}(\widetilde{g}^* - g^*)(|[\widetilde{\boldsymbol{g}}]_{g^*}|^2 - |[\widetilde{\boldsymbol{g}}]_{\widetilde{g}^*}|^2)/(|[\widetilde{\boldsymbol{g}}]_{g^*}|^2 + |[\widetilde{\boldsymbol{g}}]_{\widetilde{g}^*}|^2)$.

Note that both the beam training and the subcarrier accumulation are the DFT. Therefore, we can use (21) to improve the accuracy of (20). The estimation results of the AoD, the AoA and the delay of the LoS path for the BS-RIS link are denoted as $\widehat{\theta}_{\mathrm{BR}}$, $\widehat{\varphi}_{\mathrm{BR}}$ and $\widehat{\tau}_{\mathrm{BR}}$, respectively.

B. Target Sensing

Before performing target sensing, the echoes from the RIS need to be removed from (12), which can be formulated as

$$\min_{\alpha} \|\boldsymbol{y} - \alpha \boldsymbol{r}\|_2^2 \tag{22}$$

where

$$\begin{aligned}
&\boldsymbol{y} = [\mathrm{vec}(\boldsymbol{Y}_1)^{\mathrm{T}}, \mathrm{vec}(\boldsymbol{Y}_2)^{\mathrm{T}}, \cdots, \mathrm{vec}(\boldsymbol{Y}_{N_{\mathrm{T}}})^{\mathrm{T}}]^{\mathrm{T}},\\
&\boldsymbol{r} = [\mathrm{vec}(\boldsymbol{R}_1)^{\mathrm{T}}, \mathrm{vec}(\boldsymbol{R}_2)^{\mathrm{T}}, \cdots, \mathrm{vec}(\boldsymbol{R}_{N_{\mathrm{T}}})^{\mathrm{T}}]^{\mathrm{T}},\\
&\boldsymbol{R}_n = \xi_n \boldsymbol{F}_{N_{\mathrm{RIS}}} \boldsymbol{\alpha}(N_{\mathrm{RIS}}, 2\widehat{\varphi}_{\mathrm{BR}}) \boldsymbol{\alpha}(M, -2\widehat{\tau}_{\mathrm{BR}}\Delta f)^{\mathrm{T}},\\
&\xi_n = \boldsymbol{v}_n^{\mathrm{H}} \boldsymbol{\alpha}(N_{\mathrm{R}}, \widehat{\theta}_{\mathrm{BR}}) \boldsymbol{\alpha}(N_{\mathrm{T}}, \widehat{\theta}_{\mathrm{BR}})^{\mathrm{H}} \boldsymbol{b}_n.
\end{aligned} \tag{23}$$

The optimal solution to (22) can be expressed as $\widehat{\alpha} = \boldsymbol{r}^{\mathrm{H}}\boldsymbol{y}/(\boldsymbol{r}^{\mathrm{H}}\boldsymbol{r})$. Then, the received signals with the echoes from the RIS removed can be expressed as $\boldsymbol{T}_n^{(0)} = \boldsymbol{Y}_n - \widehat{\alpha}\boldsymbol{R}_n$. In the following, we will propose a low-complexity successive target detection algorithm to detect targets from $\boldsymbol{T}_n^{(0)}$.

To detect the lth target for $l \geq 1$, we premultiply $\boldsymbol{T}_n^{(l-1)}$ by $\boldsymbol{W}_{N_{\mathrm{RIS}}}^{\mathrm{T}}/\sqrt{N_{\mathrm{RIS}}}$ and postmultiply $\boldsymbol{T}_n^{(l-1)}$ by $\boldsymbol{F}_M$. Then, we have

$$\widetilde{\boldsymbol{T}}_n^{(l-1)} = \boldsymbol{W}_{N_{\mathrm{RIS}}}^{\mathrm{T}} \boldsymbol{T}_n^{(l-1)} \boldsymbol{F}_M = \sum_{i=l}^{T} \kappa_l \widetilde{\boldsymbol{c}}_l \widetilde{\boldsymbol{d}}_l^{\mathrm{T}} + \boldsymbol{M}_n^{(l)}, \tag{24}$$

where $\boldsymbol{M}_n^{(l)}$ denotes the noise matrix. The results of target detection can be obtained via

$$\left(n_{\mathrm{Tar}}^{(l)}, s_{\mathrm{Tar}}^{(l)}, m_{\mathrm{Tar}}^{(l)}\right) = \arg\max_{n,s,m} \left|[\widetilde{\boldsymbol{T}}_n^{(l-1)}]_{s,m}\right|. \tag{25}$$

Similar to (20), (21) can also be used to improve the accuracy of (25). The estimation results of the angle, the delay and the Doppler frequency of the lth target are denoted as $\widehat{\theta}_{\mathrm{Tar}}^{(l)}$, $\widehat{\tau}_{\mathrm{Tar}}^{(l)}$ and $\widehat{f}_{\mathrm{Tar}}^{(l)}$, respectively. Then, we remove the contribution of the lth estimated target via

$$\min_{\beta} \left\|\boldsymbol{t}^{(l-1)} - \beta \boldsymbol{s}\right\|_2^2 \tag{26}$$

where

$$\begin{aligned}
&\boldsymbol{t}^{(l-1)} = \left[\mathrm{vec}(\boldsymbol{T}_1^{(l-1)})^{\mathrm{T}}, \cdots, \mathrm{vec}(\boldsymbol{T}_{N_{\mathrm{RIS}}}^{(l-1)})^{\mathrm{T}}\right]^{\mathrm{T}},\\
&\boldsymbol{s} = \left[\mathrm{vec}(\boldsymbol{S}_1)^{\mathrm{T}}, \mathrm{vec}(\boldsymbol{S}_2)^{\mathrm{T}}, \cdots, \mathrm{vec}(\boldsymbol{S}_{N_{\mathrm{T}}})^{\mathrm{T}}\right]^{\mathrm{T}},\\
&\boldsymbol{S}_n = \varepsilon_n \boldsymbol{\alpha}\left(N_{\mathrm{RIS}}, 2\pi \widehat{f}_{\mathrm{Tar}}^{(l)} T_s\right) \boldsymbol{\alpha}\left(M, -2\widehat{\tau}_{\mathrm{Tar}}^{(l)}\Delta f\right),\\
&\varepsilon_n = \boldsymbol{v}_n^{\mathrm{H}} \boldsymbol{\alpha}\left(N_{\mathrm{R}}, \widehat{\theta}_{\mathrm{Tar}}^{(l)}\right) \boldsymbol{\alpha}\left(N_{\mathrm{T}}, \widehat{\theta}_{\mathrm{Tar}}^{(l)}\right)^{\mathrm{H}} \boldsymbol{b}_n.
\end{aligned} \tag{27}$$

The optimal solution to (26) is $\widehat{\beta} = \boldsymbol{s}^{\mathrm{H}}\boldsymbol{t}^{(l-1)}/(\boldsymbol{s}^{\mathrm{H}}\boldsymbol{s})$. Then we update $\boldsymbol{T}_n^{(l)}$ as $\boldsymbol{T}_n^{(l)} = \boldsymbol{T}_n^{(l-1)} - \widehat{\beta}\boldsymbol{S}_n$.

The procedure (24) from to (26) stops when the accumulated power of the lth target is smaller than a threshold, which can be determined referring to the criterion of the constant false alarm rate (CFAR) detector [13]. Suppose $\widehat{T}$ targets are finally detected, and the estimated parameters of the targets are denoted as $\widehat{\theta}_{\mathrm{Tar}}^{(l)}$, $\widehat{r}_{\mathrm{Tar}}^{(l)} = \widehat{\tau}_{\mathrm{Tar}}^{(l)}c/2$ and $\widehat{v}_{\mathrm{Tar}}^{(l)} = \widehat{f}_{\mathrm{Tar}}^{(l)}\lambda/2$, for $l = 1, \cdots, \widehat{T}$.

C. Beam training for the BS-UE link

We then turn to the beam alignment for the BS-UE link contained in (2). Reusing the transmitted pilots in (11), the received signals at the UE can be expressed as

$$z_{m,p} = \boldsymbol{u}_t^{\mathrm{H}}(\boldsymbol{H}_{\mathrm{c},m} + \widetilde{\boldsymbol{H}}_{\mathrm{c},m}\boldsymbol{\Phi}_p\boldsymbol{G}_{\mathrm{T},m})\boldsymbol{b}_n + \boldsymbol{u}_t^{\mathrm{H}}\boldsymbol{\eta}_{\mathrm{c}}, \tag{28}$$

where $n \in \{1, 2, \cdots N_{\mathrm{T}}\}$, $t \in \{1, 2, \cdots, N_{\mathrm{UE}}\}$ and $p = (n-1)N_{\mathrm{RIS}} + t$. Suppose $N_{\mathrm{RIS}} \geq N_{\mathrm{UE}} + 2$, we have the following two findings: 1) For each transmit beam, only N_{UE} out of N_{RIS} training symbols are used to perform the beam training between the BS and the UE. 2) The received signals at the UE contain both the signals from the BS and the signals reflected from the RIS. The first finding inspires us to think about how to use the remaining $N_{\mathrm{RIS}} - N_{\mathrm{UE}}$ training symbols, and the second finding inspires us to think about how to find out whether the training result is the direct path from the BS or the reflected path from the RIS. In the following, we will try to utilize two of the remaining training pilots to distinguish the direct path from the reflected path.

Suppose $\widehat{n}_{\mathrm{UE}}$, $\widehat{t}_{\mathrm{UE}}$ and $\widehat{p}_{\mathrm{UE}}$ denote the index of the best codeword in $\boldsymbol{\mathcal{B}}$, the index of the best codeword in $\boldsymbol{\mathcal{U}}$ and the corresponding index of training symbol, respectively. If $\widehat{n}_{\mathrm{UE}}$, $\widehat{t}_{\mathrm{UE}}$ and $\widehat{p}_{\mathrm{UE}}$ are the training results for the reflected path from the RIS, then we have

$$z_{m,\widehat{p}_{\mathrm{UE}}} \approx \boldsymbol{u}_{\widehat{t}_{\mathrm{UE}}}^{\mathrm{H}} \widetilde{\boldsymbol{H}}_{\mathrm{c},m} \boldsymbol{\Phi}_{\widehat{p}_{\mathrm{UE}}} \boldsymbol{G}_{\mathrm{T},m} \boldsymbol{b}_{\widehat{n}_{\mathrm{UE}}} + \boldsymbol{u}_{\widehat{t}_{\mathrm{UE}}}^{\mathrm{H}} \boldsymbol{\eta}_{\mathrm{c}}, \tag{29}$$

where we omit the channel from the BS and the noise term. For the $(\widehat{p}_{\mathrm{UE}} + 2)$th transmit symbol, the transceiver still transmits the pilot with $\boldsymbol{b}_{\widehat{n}_{\mathrm{UE}}}$ according to (11) and the UE still receives the pilot with $\boldsymbol{u}_{\widehat{t}_{\mathrm{UE}}}$, while the RIS reflects the signal with $\boldsymbol{\Phi}_{\widehat{p}_{\mathrm{UE}}+2}$. Then, the received signal at the UE can be expressed as

$$z_{m,\widehat{p}_{\mathrm{UE}}+2} \approx \boldsymbol{u}_{\widehat{t}_{\mathrm{UE}}}^{\mathrm{H}} \widetilde{\boldsymbol{H}}_{\mathrm{c},m} \boldsymbol{\Phi}_{\widehat{p}_{\mathrm{UE}}+2} \boldsymbol{G}_{\mathrm{T},m} \boldsymbol{b}_{\widehat{n}_{\mathrm{UE}}} + \boldsymbol{u}_{\widehat{t}_{\mathrm{UE}}}^{\mathrm{H}} \boldsymbol{\eta}_{\mathrm{c}}. \tag{30}$$

Based on (29) and (30), we have

$$\rho = |z_{m,\widehat{p}_{\mathrm{UE}}+2}|/|z_{m,\widehat{p}_{\mathrm{UE}}}| \approx 0 \tag{31}$$

due to the power difference between the beam alignment and beam misalignment. On the other hand, If $\widehat{n}_{\mathrm{UE}}$, $\widehat{t}_{\mathrm{UE}}$ and $\widehat{p}_{\mathrm{UE}}$ are the training results for the direct path, we have

$$\begin{aligned}
&z_{m,\widehat{p}_{\mathrm{UE}}} \approx \boldsymbol{u}_{\widehat{t}_{\mathrm{UE}}}^{\mathrm{H}} \boldsymbol{H}_{\mathrm{c},m} \boldsymbol{b}_{\widehat{n}_{\mathrm{UE}}} + \boldsymbol{u}_{\widehat{t}_{\mathrm{UE}}}^{\mathrm{H}} \boldsymbol{\eta}_{\mathrm{c}},\\
&z_{m,\widehat{p}_{\mathrm{UE}}+2} \approx \boldsymbol{u}_{\widehat{t}_{\mathrm{UE}}}^{\mathrm{H}} \boldsymbol{H}_{\mathrm{c},m} \boldsymbol{b}_{\widehat{n}_{\mathrm{UE}}} + \boldsymbol{u}_{\widehat{t}_{\mathrm{UE}}}^{\mathrm{H}} \boldsymbol{\eta}_{\mathrm{c}}.
\end{aligned} \tag{32}$$

$$\rho = |z_{m,\widehat{p}_{\mathrm{UE}}+2}|/|z_{m,\widehat{p}_{\mathrm{UE}}}| \approx 1. \tag{33}$$

Note that the value of ρ in (33) differs from that in (31) lies in the fact that the beam training in (11) is dedicated to the BS-RIS link and the BS-UE link instead of the BS-RIS-UE link. Exploiting the difference between (31) and (33), we only need two more time slots to identify whether the training results correspond to the direct path from the BS or the reflected path from the RIS.

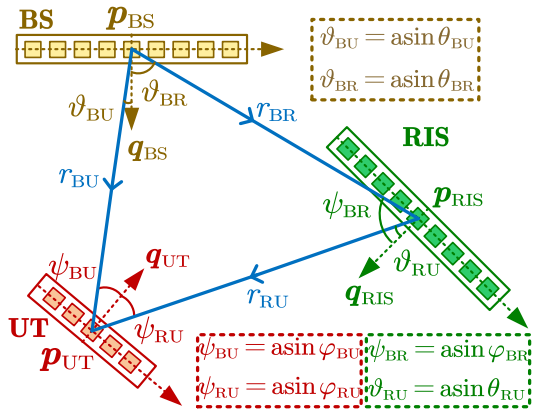

Fig. 2. The geometry relation between the BS, the RIS and the UE

For the nth transmit beam, we stack the received signals at the M subcarriers for the N_{UE} received beams together as $\boldsymbol{Z}_n \in \mathbb{C}^{N_{\mathrm{UE}} \times M}$. Similar to (14), we postmultiply $\boldsymbol{Z}_n$ with $\boldsymbol{F}_{\mathrm{M}}$ for subcarrier accumulation, and obtain $\widetilde{\boldsymbol{Z}}_n = \boldsymbol{Z}_n \boldsymbol{F}_{\mathrm{M}}$. The training results are obtained via

$$(\widehat{n}_{\mathrm{UE}}, \widehat{t}_{\mathrm{UE}}, \widehat{m}_{\mathrm{UE}}) = \arg \max_{n,t,m} \left| [\widetilde{\boldsymbol{Z}}_n]_{t,m} \right|. \tag{34}$$

If ρ calculated from (31) or (33) is bigger than the predefined threshold, such as 0.5, then $n^*_{\mathrm{UE}} = \widehat{n}_{\mathrm{UE}}$, $t^*_{\mathrm{UE}} = \widehat{t}_{\mathrm{UE}}$ and $m^*_{\mathrm{UE}} = \widehat{m}_{\mathrm{UE}}$ are termed as the training results for the BS-UE link. Otherwise, we refind n^*_{UE}, t^*_{UE} and m^*_{UE} via

$$(n^*_{\mathrm{UE}}, t^*_{\mathrm{UE}}, m^*_{\mathrm{UE}}) = \arg \max_{\substack{n,t,m, n \neq \widehat{n}_{\mathrm{UE}} \\ t \neq \widehat{t}_{\mathrm{UE}}, m \neq \widehat{m}_{\mathrm{UE}}}} \left| [\widetilde{\boldsymbol{Z}}_n]_{t,m} \right|. \tag{35}$$

Then, similar to (20), we can also use (21) to improve the estimation accuracy of (35). The estimation results of the AoD, the AoA and the delay of the LoS path for the BS-UE link are denoted as $\widehat{\theta}_{\mathrm{BU}}$, $\widehat{\varphi}_{\mathrm{BU}}$ and $\widehat{\tau}_{\mathrm{BU}}$, respectively.

D. Beam alignment for the RIS-UE link

As shown in Fig. 2, we illustrate the geometry relation between the antenna arrays at the BS, the RIS and the UE. Note that we have obtained $\widehat{\theta}_{\mathrm{BR}}$, $\widehat{\varphi}_{\mathrm{BR}}$ as well as $\widehat{r}_{\mathrm{BR}} = \widehat{\tau}_{\mathrm{BR}} c$ in Section III-A and have obtained $\widehat{\theta}_{\mathrm{BU}}$, $\widehat{\varphi}_{\mathrm{BU}}$ as well as $\widehat{r}_{\mathrm{BU}} = \widehat{\tau}_{\mathrm{BU}} c$ in Section III-C. To establish the link between the RIS and the UE, we only need to obtain $\widehat{\theta}_{\mathrm{RU}}$ and $\widehat{\varphi}_{\mathrm{RU}}$.

According to the geometry relation in Fig. 2, the positions of the BS, the RIS and the UE can be expressed as

$$\begin{aligned} \boldsymbol{p}_{\mathrm{BS}} &= [0,0]^{\mathrm{T}}, \ \boldsymbol{p}_{\mathrm{RIS}} = -\widehat{r}_{\mathrm{BR}} \left[\widehat{\theta}_{\mathrm{BR}}, \sqrt{1-\widehat{\theta}^2_{\mathrm{BR}}} \right]^{\mathrm{T}}, \\ \boldsymbol{p}_{\mathrm{UE}} &= -\widehat{r}_{\mathrm{UE}} \left[\widehat{\varphi}_{\mathrm{UE}}, \sqrt{1-\widehat{\varphi}^2_{\mathrm{UE}}} \right]^{\mathrm{T}}. \end{aligned} \tag{36}$$

The normal directions of the antenna arrays at the RIS and the UE can be expressed as

$$\begin{aligned} \boldsymbol{q}_{\mathrm{RIS}} &= \begin{bmatrix} \sqrt{1-\widehat{\varphi}^2_{\mathrm{BR}}} & -\widehat{\varphi}_{\mathrm{BR}} \\ \varphi_{\mathrm{BR}} & \sqrt{1-\widehat{\varphi}^2_{\mathrm{BR}}} \end{bmatrix} \frac{\boldsymbol{p}_{\mathrm{BS}} - \boldsymbol{p}_{\mathrm{RIS}}}{\|\boldsymbol{p}_{\mathrm{BS}} - \boldsymbol{p}_{\mathrm{RIS}}\|_2}, \\ \boldsymbol{q}_{\mathrm{UE}} &= \begin{bmatrix} \sqrt{1-\widehat{\varphi}^2_{\mathrm{BU}}} & -\widehat{\varphi}_{\mathrm{BU}} \\ \varphi_{\mathrm{BU}} & \sqrt{1-\widehat{\varphi}^2_{\mathrm{BU}}} \end{bmatrix} \frac{\boldsymbol{p}_{\mathrm{BS}} - \boldsymbol{p}_{\mathrm{UE}}}{\|\boldsymbol{p}_{\mathrm{BS}} - \boldsymbol{p}_{\mathrm{UE}}\|_2}. \end{aligned} \tag{37}$$

Define $\boldsymbol{l} \triangleq (\boldsymbol{p}_{\mathrm{RIS}} - \boldsymbol{p}_{\mathrm{UE}})/\|\boldsymbol{p}_{\mathrm{RIS}} - \boldsymbol{p}_{\mathrm{UE}}\|_2$. Then, $\widehat{\theta}_{\mathrm{RU}}$ and $\widehat{\varphi}_{\mathrm{RU}}$ can be expressed as

$$\begin{aligned} \widehat{\theta}_{\mathrm{RU}} &= -([\boldsymbol{q}_{\mathrm{RIS}}]_2 - [\boldsymbol{l}]_2 \boldsymbol{l}^{\mathrm{T}} \boldsymbol{q}_{\mathrm{RIS}})/[\boldsymbol{l}]_1, \\ \widehat{\varphi}_{\mathrm{RU}} &= ([\boldsymbol{q}_{\mathrm{UE}}]_2 - [\boldsymbol{l}]_2 \boldsymbol{l}^{\mathrm{T}} \boldsymbol{q}_{\mathrm{UE}})/[\boldsymbol{l}]_1. \end{aligned} \tag{38}$$

Finally, we summarize the steps of the proposed simultaneous beam training and target sensing scheme in **Algorithm 1**.

Algorithm 1 Simultaneous Beam Training and Target Sensing

1: **Input:** N_{T}, N_{R}, N_{RIS}, N_{UE}, M, Δf, T_{s}, $\boldsymbol{\mathcal{B}}$, $\boldsymbol{\mathcal{U}}$, $\boldsymbol{\mathcal{R}}$.
2: **BS-RIS-BS link:**
3: Obtain $\widehat{\theta}_{\mathrm{BR}}$, $\widehat{\varphi}_{\mathrm{BR}}$ and $\widehat{\tau}_{\mathrm{BR}}$ via (20) and (21).
4: **Target Sensing:**
5: Obtain $\widehat{\theta}^{(l)}_{\mathrm{Tar}}$, $\widehat{r}^{(l)}_{\mathrm{Tar}}$ and $\widehat{v}^{(l)}_{\mathrm{Tar}}$, for $l = 1, \cdots, \widehat{T}$ via (25).
6: **BS-UE link:**
7: Obtain $\widehat{\theta}_{\mathrm{BU}}$, $\widehat{\varphi}_{\mathrm{BU}}$ and $\widehat{\tau}_{\mathrm{BU}}$ via (34), (35) and (21).
8: **RIS-UE link:**
9: Obtain $\widehat{\theta}_{\mathrm{RU}}$ and $\widehat{\varphi}_{\mathrm{RU}}$ via (38).
10: **Output:** $\widehat{\theta}_{\mathrm{BR}}$, $\widehat{\varphi}_{\mathrm{BR}}$, $\widehat{\theta}_{\mathrm{BU}}$, $\widehat{\varphi}_{\mathrm{BU}}$, $\widehat{\theta}_{\mathrm{RU}}$ and $\widehat{\varphi}_{\mathrm{RU}}$; $\widehat{\theta}^{(l)}_{\mathrm{Tar}}$, $\widehat{r}^{(l)}_{\mathrm{Tar}}$ and $\widehat{v}^{(l)}_{\mathrm{Tar}}$, for $l = 1, \cdots, \widehat{T}$.

IV. Simulation Results

Now we evaluate the performance of the proposed simultaneous beam training and target sensing scheme. We consider an ISAC BS employing a transceiver with $N_{\mathrm{T}} = 32$ antennas and a receiver with $N_{\mathrm{R}} = 32$ antennas. The number of elements at the RIS is set to be 128. The carrier frequency is set to be 26.5 GHz. OFDM is adopted for wideband processing, where the number of subcarriers is set to be $M = 128$ and the subcarrier spacing is set to be $\Delta f = 120$ KHz. To compare different systems fairly, we adopt the widely-used free space propagation model to characterize the path loss [14], where we set $L_{\mathrm{BR}} = 3$, $L_{\mathrm{BU}} = 3$, $r^{(l)}_{\mathrm{BS}} \sim U(20, 40)$ m, $r^{(l)}_{\mathrm{Tar}} \sim U(50, 150)$ m and $r^{(l)}_{\mathrm{UE}} \sim U(50, 150)$ m. The noise power at both the receiver and the UE is set to be -103 dBm. The number of targets is set to be $T = 4$ and the radar cross section (RCS) of targets distributes randomly within $[0.1, 1]$ m^2. The ratio of the LoS path power to the NLoS path power is set to be 20 dB.

In Fig. 3, we illustrate the positioning error for different equipment including the UE, the targets and the RIS under different transmit power of each subcarrier. To demonstrate the interference between the targets and the RIS, the positioning error of the RIS without interference cancellation (wIC) is adopted as a benchmark. Define the real position of an equipment and its estimation as $\boldsymbol{p}$ and $\widehat{\boldsymbol{p}}$, respectively. Then, the positioning error is defined as $E \triangleq \|\boldsymbol{p} - \widehat{\boldsymbol{p}}\|_2$. It is

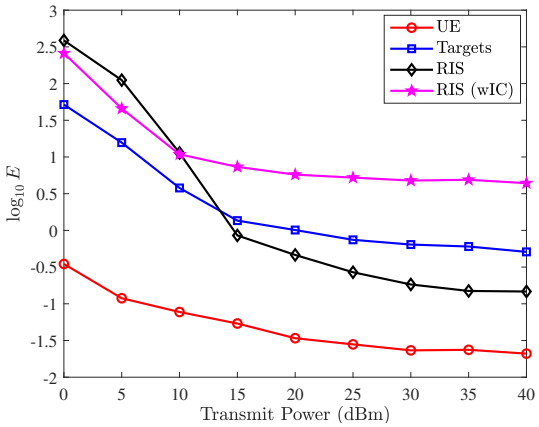

Fig. 3. Comparisons of the positioning error for different equipment.

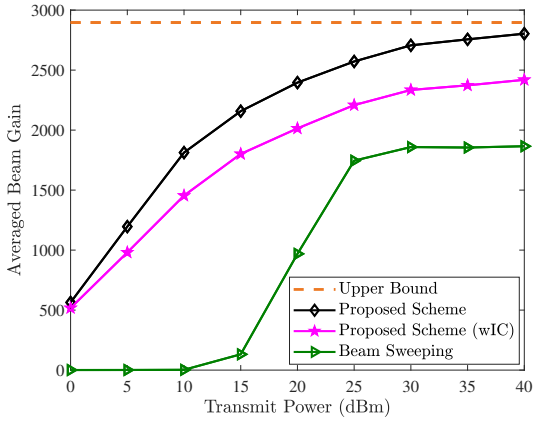

Fig. 4. Comparisons of the beamforming gains for different schemes.

shown that the UE has the smallest positioning error among all the equipment because the positioning of UE relies on the directly propagated signal while the positioning of other two equipment relies on the reflected propagating signal. It is well-known that, for fixed distance, the former usually has larger received signal-to-noise-ratio (SNR) than the latter. It is also shown that the targets have better positioning performance than the RIS for small transmit power. That is because CFAR detector is integrated to the target sensing, which enables the target sensing to avoid the false detection caused by the noise. On the contrary, the RIS has better positioning performance than the targets for large transmit power. That is because the RIS is set to be closer to the BS than the targets, which leads to smaller positioning error for a fixed angle error. Finally, the RIS has much better positioning performance if interference cancellation is performed, which further verifies the effectiveness of the proposed scheme.

In Fig. 4, we compare the beamforming gains of the BS-RIS-UE link after beam alignment for different schemes. It is shown that, the proposed scheme performs much better than the beam sweeping. For low transmit power, the superiority of the proposed scheme comes from the shorter distance between the BS and the RIS, which results in larger received SNRs. For high transmit power, the superiority of the proposed scheme comes from the accurate positioning of the RIS and the UE, which results in more accurate beam alignment than rough beam sweeping. Note that the proposed scheme needs $N_{\mathrm{T}}N_{\mathrm{RIS}}$ times of beam training while the beam sweeping needs $N_{\mathrm{T}}N_{\mathrm{RIS}}N_{\mathrm{UE}}$ times of beam training, where the former is much smaller than the latter especially when N_{UE} is large.

V. Conclusion

In this paper, we have proposed a simultaneous beam training and target sensing scheme for the RIS-aided ISAC systems. Future works will be continued by exploiting sensing to enhance wireless communication.

VI. Acknowledgment

This work is supported in part by National Natural Science Foundation of China (NSFC) under Grant U22B2007 and 62071116, and by National Key Research and Development Program of China under Grant 2021YFB2900404.

References

[1] J. A. Zhang, M. L. Rahman, K. Wu *et al.*, "Enabling joint communication and radar sensing in mobile networks—A survey," *IEEE Commun. Surv. Tut.*, vol. 24, no. 1, pp. 306–345, Oct. 2021.

[2] C. Qi, W. Ci, J. Zhang *et al.*, "Hybrid beamforming for millimeter wave MIMO integrated sensing and communications," *IEEE Commun. Lett.*, vol. 26, no. 5, pp. 1136–1140, May 2022.

[3] F. Liu, Y. Cui, C. Masouros *et al.*, "Integrated sensing and communications: Toward dual-functional wireless networks for 6G and beyond," *IEEE J. Sel. Areas Commun.*, vol. 40, no. 6, pp. 1728–1767, Mar. 2022.

[4] C. Qi, P. Dong, W. Ma *et al.*, "Acquisition of channel state information for mmWave massive MIMO: Traditional and machine learning-based approaches," *Sci. China Inf. Sci.*, vol. 64, no. 8, p. 181301, Aug. 2021.

[5] Z. Wang, L. Liu, and S. Cui, "Channel estimation for intelligent reflecting surface assisted multiuser communications: Framework, algorithms, and analysis," *IEEE Trans. Wireless Commun.*, vol. 19, no. 10, pp. 6607–6620, June 2020.

[6] D. Mishra and H. Johansson, "Channel estimation and low-complexity beamforming design for passive intelligent surface assisted MISO wireless energy transfer," in *Proc. IEEE Int. Conf. Acoust., Speech Signal Process. (ICASSP)*, Brighton, UK, May 2019, pp. 4659–4663.

[7] P. Wang, J. Fang, W. Zhang *et al.*, "Beam training and alignment for RIS-assisted millimeter wave systems: State of the art and beyond," *IEEE Wireless Commun.*, vol. 29, no. 6, pp. 64–71, Dec. 2022.

[8] Z.-M. Jiang, M. Rihan, P. Zhang *et al.*, "Intelligent reflecting surface aided dual-function radar and communication system," *IEEE Syst. J.*, vol. 16, no. 1, pp. 475–486, Feb. 2022.

[9] R. Liu, M. Li, Y. Liu *et al.*, "Joint transmit waveform and passive beamforming design for RIS-aided DFRC systems," *IEEE J. Sel. Top. Signal Process.*, vol. 16, no. 5, pp. 995–1010, May 2022.

[10] C. Qi, K. Chen, O. A. Dobre, and G. Y. Li, "Hierarchical codebook-based multiuser beam training for millimeter wave massive MIMO," *IEEE Trans. Wireless Commun.*, vol. 19, no. 12, pp. 8142–8152, Sep. 2020.

[11] K. Chen, C. Qi, and G. Y. Li, "Two-step codeword design for millimeter wave massive MIMO systems with quantized phase shifters," *IEEE Trans. Signal Process.*, vol. 68, pp. 170–180, Jan. 2020.

[12] D. Zhu, J. Choi, and R. W. Heath, "Auxiliary beam pair enabled AoD and AoA estimation in closed-loop large-scale millimeter-wave MIMO systems," *IEEE Trans. Wireless Commun.*, vol. 16, no. 7, pp. 4770–4785, July 2017.

[13] M. A. Richards, *Fundamentals of Radar Signal Processing*, 2nd ed. New York, NY, USA: McGraw-Hill, 2005.

[14] X. Shao, C. You, W. Ma *et al.*, "Target sensing with intelligent reflecting surface: Architecture and performance," *IEEE J. Sel. Areas Commun.*, vol. 40, no. 7, pp. 2070–2084, Mar. 2022.